

Erney, L.M.A.G.

~~144-6410~~  
~~62~~  
~~PT 1~~  
~~48~~  
~~C~~

TECHNICAL MEMORANDUMS  
NATIONAL ADVISORY COMMITTEE FOR AERONAUTICS

-----  
No. 822  
-----

TURBULENT BOUNDARY LAYER OF AN AIRFOIL

By K. Fediaevsky

Central Aero-Hydrodynamical Institute

-----  
Washington  
April 1937



## NATIONAL ADVISORY COMMITTEE FOR AERONAUTICS

TECHNICAL MEMORANDUM NO. 822

## TURBULENT BOUNDARY LAYER OF AN AIRFOIL\*

By K. Fediaevsky

1. All the work that has been published up to the present on the turbulent boundary layer is based, as we know, on the application of the velocity distributions theoretically or semi-empirically derived either for the case of the motion of a fluid in straight round pipes, i.e., for the case of linear distribution of the frictional shear across the boundary layer (exponential law, logarithmic law of von Kármán), or for the case of the motion of a fluid with constant shear across the boundary layer (logarithmic law of Prandtl-Nikuradse). It is evident that neither of the above shear distributions corresponds to the case of flow about a curvilinear contour and that the velocity profiles do not take into account, for example, the effect of the static pressure gradient which, in the solution of several very important problems, for example, that of the separation of flow at the turbulent boundary layer of a wing, is a factor of greater importance than surface friction in its effect on the boundary layer. In such cases as these the correctness of employing the velocity distributions that were theoretically obtained for other shearing stress distributions may be questioned. } good

Experiment shows, in fact, that in a boundary layer with positive or negative pressure gradient, the velocity distribution differs considerably from that obtaining in a straight round pipe.

On figures 1, 2, and 3 are shown velocity-distribution curves in boundary layers as obtained from the tests of Gruschwitz (reference 5). The curves are given in non-dimensional coordinates, the velocity  $U$  being expressed in terms of the velocity  $U_0$  at the outer limit of the boundary layer, and the distance  $y$  to the wall in terms of the boundary-layer thickness  $\delta$ . For comparison, the curve of distribution according to the one-seventh power law is also given. We see that for a positive static pressure gradient in the boundary layer of a wing (fig. 1) or in a plane diffuser (fig. 2) the velocities fall con-

\*Report No. 282, of the Central Aero-Hydrodynamical Institute, Moscow, 1936.

siderably more rapidly as the wall is approached than is indicated by the seventh power law. Conversely, for a negative static pressure gradient in the boundary layer of a wing or plane converging passage (fig. 3) the velocities, as the wall is approached, fall less rapidly than the seventh power law would indicate. It is seen, moreover, that even for an approximately constant pressure gradient the velocity profiles are not at all similar to one another. A glance at figures 1, 2, and 3 shows that the farther along the flow the cross section under consideration lies, the more do the velocity profiles deviate from the seventh-power law.

The above character of the velocity distribution is also evidenced by diverging or converging passages with plane walls beyond the "anlaufstrecke" (the initial portion), i. e., when the entire cross section of the diffuser is taken up by the boundary layer. This is confirmed by the experimental results of Doench (reference 2) and Nikuradse (reference 7).

All that has been said above indicates the need for a new determination of the velocity profiles in the boundary layer. Assuming that the character of the velocity distribution depends to a large extent on the character of the shear distribution across the boundary layer, we shall consider the nature of the shear distribution for a boundary layer with a pressure gradient.

2. The shear stress in the turbulent boundary layer, in terms of the shear at the wall, we shall present in the form of a power series

$$\frac{\tau}{\tau_0} = A_0 + A_1 \left(\frac{y}{\delta}\right) + A_2 \left(\frac{y}{\delta}\right)^2 + A_3 \left(\frac{y}{\delta}\right)^3 + A_4 \left(\frac{y}{\delta}\right)^4 + \dots \quad (1)$$

the constants of which are determined by the conditions obtaining at the outer limit of the boundary layer, for the values of  $\tau/\tau_0$  and its derivatives. For a number of terms of the series up to the fourth power term, there are a sufficient number of such conditions for the determination of the constants. These conditions are as follows:

I. At the wall, i. e., for  $y = 0$  the ratio  $\left[\frac{\tau}{\tau_0}\right]_{y=0} = 1$ . (I)

II. The differential equation of an element of a tube of flow in the boundary layer of a two-dimensional flow

may be written, if we neglect the term due to the curvature of the element, in the form

$$\rho V \frac{\partial V}{\partial S} = - \frac{\partial p}{\partial S} + \frac{\partial \tau}{\partial n} \quad (2)$$

where  $\rho$  is the density of the fluid

$V$ , the velocity

$S$ , length measured along a streamline

$p$ , static pressure

$n$ , length measured along normal to streamline

Since near the surface of the body the normals to the streamlines differ but little in direction from the normals to the surface of the body we may, in equation (2), substitute  $\partial \tau / \partial y$  for  $\partial \tau / \partial n$  where  $y$  is measured along the normal to the surface. Equation (2) then assumes the following form:

$$\rho V \frac{\partial V}{\partial S} = - \frac{\partial p}{\partial S} + \frac{\partial \tau}{\partial y} \quad (2')$$

At  $y = 0$  the left-hand member of (2') becomes zero so that  $\partial \tau / \partial y = \partial p / \partial S$  and therefore,

$$\left[ \frac{\partial \left( \frac{\tau}{\tau_0} \right)}{\partial \left( \frac{y}{\delta} \right)} \right]_{y=0} = \frac{\delta}{\tau_0} \frac{\partial p}{\partial S} \quad (II)$$

III. At the outer edge of the boundary layer, i.e., at  $y = \delta$

$$\left[ \frac{\tau}{\tau_0} \right]_{y=\delta} = 0 \quad (III)$$

by the very definition of boundary layer.

IV. Assuming that the derivative of the total head

$$\frac{\rho V^2}{2 + p} \quad \frac{1}{2} \rho V^2 + p.$$

of the fluid suffers no discontinuity at the outer edge of the boundary layer (as is confirmed by experiments) and

noting that outside the boundary layer

$$\frac{\partial}{\partial s} \left( \frac{\rho V^2}{2} + p \right) = \rho V \frac{\partial V}{\partial s} + \frac{\partial p}{\partial s} = 0$$

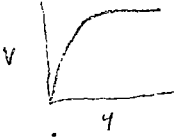
we obtain from equation (2'), for  $y = \delta$

$$\frac{\partial \tau}{\partial y} = \rho V \frac{\partial V}{\partial s} + \frac{\partial p}{\partial s} = 0$$

and therefore,

$$\left[ \frac{\partial \left( \frac{\tau}{\tau_0} \right)}{\partial \left( \frac{y}{\delta} \right)} \right]_{y=\delta} = 0 \quad (\text{IV})$$

V. Differentiating equation (2') with respect to  $y$ , we have:



$$\rho \left[ \frac{\partial V}{\partial y} \frac{\partial V}{\partial s} + v \frac{\partial}{\partial y} \left( \frac{\partial V}{\partial s} \right) \right] = \frac{\partial^2 \tau}{\partial y^2} \quad (3)$$

since, according to the second of Prandtl's boundary layer differential equations the pressure is constant transverse to the layer. At the wall, i.e., at  $y = 0$ , the left-hand member of equation (3) becomes zero so that

$$\left( \frac{\partial^2 \tau}{\partial y^2} \right)_{y=0} = 0 =$$

and therefore,

$$\left[ \frac{\partial^2 \left( \frac{\tau}{\tau_0} \right)}{\partial \left( \frac{y}{\delta} \right)^2} \right]_{y=0} = 0 \quad (\text{V})$$

The above conditions can also be obtained by considering the differential equations of Prandtl.

The idea of representing the shear stress in the boundary layer in the form of a polynomial was first suggested, as far as is known to the author, by Buri in 1931. (See reference 1.) Buri, however, proposed the series

$$\frac{\tau}{\tau_0} = 1 + \Gamma_a \left(\frac{y}{\theta}\right) + \Gamma_b \left(\frac{y}{\theta}\right)^2 + \dots$$

where  $\theta$  is the so-called "momentum loss length," i.e., a linear magnitude proportional to the loss of momentum in the boundary layer, its value being defined by the formula

$$\theta = \int_0^{\delta} \frac{U}{U_{\delta}} \left(1 - \frac{U}{U_{\delta}}\right) dy = \frac{1}{U_{\delta}^2} \int_0^{\delta} (UU_{\delta} - U^2) dy$$

We thus see that  $\theta$  is, in fact, a magnitude proportional to the difference between the momentum of the fluid mass flowing through the boundary layer with the velocity of the outer edge of the layer and the actual momentum within the boundary layer.

The coefficients of the polynomial proposed by Buri, however, cannot be determined since the shear stress and its derivatives can be evaluated only from the conditions at the wall, i.e., for  $y/\theta = 0$ . But of these conditions of Buri, only numbers (I) and (II) were made use of. Thus, the expression proposed by Buri does not enable the shear stress distribution across the boundary layer to be determined and could not therefore be employed by him.

We shall determine the coefficients of the polynomial from our conditions given above:

a) Using conditions (I), (II), (III), (IV), and (V), we have

$$\left. \begin{aligned} A_0 &= 1; & A_1 &= \frac{\delta}{\tau_0} \frac{\partial p}{\partial s}; & A_2 &= 0 \\ A_3 &= -4 - 3 \frac{\delta}{\tau_0} \frac{\partial p}{\partial s}; & A_4 &= 3 + 2 \frac{\delta}{\tau_0} \frac{\partial p}{\partial s} \end{aligned} \right\} \quad (4)$$

b) Using conditions (I), (II), (III), and (IV), we have

$$\left. \begin{aligned} A_0 &= 1; & A_1 &= \frac{\delta}{\tau_0} \frac{\partial p}{\partial s} \\ A_2 &= -3 - 2 \frac{\delta}{\tau_0} \frac{\partial p}{\partial s}; & A_3 &= 2 + \frac{\delta}{\tau_0} \frac{\partial p}{\partial s} \end{aligned} \right\} \quad (5)$$

c) Using conditions (I), (II), and (III), we have

$$A_0 = 1; \quad A_1 = \frac{\delta}{\tau_0} \frac{\partial p}{\partial S}; \quad A_2 = -1 - \frac{\delta}{\tau_0} \frac{\partial p}{\partial S} \quad (6)$$

It should first of all be noted that conditions (I), (II), (III), (IV), and (V) apply equally well to both the laminar and turbulent boundary flow so that for the same values of the magnitude  $\frac{\delta}{\tau_0} \frac{\partial p}{\partial S}$  the nondimensional shear distribution may be considered to be the same for both the laminar and turbulent flow with the same degree of accuracy with which the series (1) represents the actual shear distribution. Unfortunately, we have no means at present of estimating the degree of approximation of the interpolation formula employed by us. For this reason, the choice of one or the other combination of conditions can for the present be decided only on the basis of the best agreement between the values of the shear forces and velocities as obtained from any one of the combinations of conditions with the corresponding values as obtained from experiment.

The character of the <sup>turbulent shear profiles</sup> shear profiles obtained for a positive pressure gradient is confirmed by the tests of Gruschwitz. On figure 5 are shown the shear profiles for four sections of the boundary layer of a wing for an angle of attack of  $12^\circ$  as obtained by Gruschwitz. The absolute values of the shear differ somewhat from those obtained by our computations. We assume that this can be explained only as due to the very great inaccuracy in the experimental determination of the shear (as brought out by Gruschwitz himself in his paper). In the experimental determination of the shear, it is necessary to differentiate graphically the total head of the fluid along a streamline. On account of the small number of cross sections at which the total head was measured in the tests of Gruschwitz such differentiation may, to a large extent, be arbitrary.

It is necessary therefore that the choice of one or the other of the combinations of conditions for the determination of the constants of the series be made for the present only on the basis of the best agreement between the values of the velocities as obtained from any one of the combination of conditions with the values obtained by experiment since the experimental determination of the velocities in the boundary layer is much more accurate than the experimental determination of the shear stresses.

Figure 4 gives the nondimensional shear profiles for the cases  $\frac{\partial p}{\partial S} > 0$  and  $\frac{\partial p}{\partial S} = 0$ , respectively. The profiles are drawn on the basis of the two combinations of conditions (I), (II), (III); and (I), (II), (III), (IV), (V), respectively. We see that even the combination of the three conditions (I), (II), and (III) determines in general the character of the shear profile.

It is interesting to note that the profile for the case of a flat plate, i. e., for  $\partial p / \partial S = 0$  does not differ from the straight line shear profile of a straight round pipe to the same extent as does the profile for the case  $\frac{\partial p}{\partial S} > 0$ . It is thus understandable why, for a condition where  $\frac{\partial p}{\partial S}$  is near or equal to zero (dirigible body, flat plate) the use of the velocity profiles obtained for straight round pipes yields comparatively good results.

3. To obtain the velocity distribution it is possible, first of all, to integrate equation (2') along a streamline. For this purpose we shall write equation (2') in the following form:

$$\frac{\partial}{\partial S} \left( \frac{\rho V^2}{2} \right) + \frac{\partial p}{\partial S} = \frac{\partial \tau}{\partial y} \quad (2'')$$

Integrating with respect to  $S$ , we arrive of course at the equation of Bernoulli with the energy loss due to the internal friction taken into account:

$$\frac{\rho V^2}{2} + p = \frac{\rho V_0^2}{2} + p_0 + \int_0^S \frac{\partial \tau}{\partial y} ds \quad (7)$$

where the subscript denotes some initial point on the streamline,  $V_0$  and  $p_0$  being the velocity and static pressure, respectively, at this point.

The expression for the shear, bearing in mind the value of the coefficient  $A_0$ , may be written in the following form:

$$\begin{aligned} \tau &= \frac{\tau}{\tau_0} \tau_0 = \left[ 1 + A_1 \left( \frac{y}{\delta} \right) + A_2 \left( \frac{y}{\delta} \right)^2 + \dots - \right] \tau_0 = \\ &= \tau_0 + A_1 \frac{\tau_0}{\delta} y + A_2 \frac{\tau_0}{\delta^2} y^2 + \dots = \tau_0 + \frac{\partial p}{\partial S} y + a_2 y^2 + a_3 y^3 + \dots \quad (8) \end{aligned}$$

Differentiating  $\tau$  with respect to  $y$ , we have:

$$\frac{\partial \tau}{\partial y} = \frac{\partial p}{\partial s} + 2a_2y + 3a_3y^2 + \dots \quad (9)$$

Substituting (9) in (7) and integrating the first term in the expression under the integral sign, we obtain:

$$\frac{\rho V^2}{2} = \frac{\rho V_0^2}{2} + \int_0^s (2a_2y + 3a_3y^2 + \dots) ds \quad (10)$$

Formula (10) enables the change in velocity along a streamline to be computed if the change in the ordinate  $y$  along a streamline and the velocity at the initial section are given. For the latter, at which the velocity distribution may be assumed to follow the exponential or logarithmic law, the cross section at some initial point at the beginning of the turbulent boundary layer may be taken. The nearer this section is taken to the starting point of the turbulent boundary layer the smaller will be the portion of the profile where the inaccuracy of the initial profile will show up. The thickness of the boundary layer and shear at the wall are determined by employing the exponential or logarithmic law.

To determine the variation of the coordinate  $y$  along a streamline, it is necessary to define a line of flow at least to a first approximation. For this purpose, we shall assume some known velocity distribution (the exponential law is best on account of its simplicity) and define lines of flow as those at which

$$\int_0^y U dy = \text{const} \quad (11)$$

where  $U$  is the tangential component of the velocity.

Setting up the velocity distribution in this manner to a first approximation, more accurate lines of flow may be determined to a second degree of approximation by using condition (11) for the obtained velocity distribution. Using the lines of flow of the second approximation, a more accurate velocity distribution to a second approximation may be computed, etc. On account of the extreme cumbersomeness of the above method, however, it can only be applied with difficulty. Moreover, by the above method we may compute the velocity profiles for various sections of the boundary layer but cannot establish the law of variation of the velocity across the boundary layer.

4. In order to establish the law of variation of the velocity across the boundary layer, it is necessary to assume some form of dependence between the shear and the velocity. In the case of the turbulent boundary layer, this is equivalent to the assumption of some model for the turbulence.

We shall express the shear with the aid of the Prandtl "Mischungsweg" formula:

$$\tau = \rho \, l^2 \left. \frac{dU}{dy} \right| \left. \frac{dU}{dy} \right| \quad (12)$$

where  $l$  denotes the so-called "Mischungsweg" or mixing length and represents a magnitude that is analogous to the mean free path of a molecule in the kinetic theory of gases. In turbulent flow the mixing length is a magnitude proportional to the displacements of aggregate volumes of the fluid transverse to the general flow direction. In formula (12) one of the factors  $du/dy$  is taken in the absolute sense so as to preserve the correspondence between the sign of the velocity gradient and that of the shear.

With regard to the question as to what are the variables of which the mixing length is a function, there are various views held. von Kármán assumes that the mixing length is determined by ratio of the first derivative of the velocity with respect to  $y$  to the second derivative, i.e., that the turbulence is locally defined. Prandtl, for the case where the shear across the boundary layer is constant, considers the mixing length to be determined by the distance from the wall and assumes, as a first approximation, that the mixing length is simply proportional to the distance from the wall.

In view of the essential difference in the opinions as to the nature of the mixing length, we shall turn to a consideration of what experiment has to offer with regard to this matter.

The outstanding experimental work of Nikuradse (reference 8) established the fact that in smooth round pipes at Reynolds Numbers above 100,000 the nondimensional mixing length, that is, the mixing length divided by the pipe radius  $r$  appears to be a function only of the nondimensional distance  $y/r$  from the wall and does not depend on the Reynolds Number. Figure 6 shows that the nondimensional mixing length varies with the nondimensional distance

from the wall for various Reynolds Numbers according to the tests of Nikuradse. The Reynolds Number  $Re$  is here computed from the pipe diameter and mean velocities. The form of dependence shown on figure 6 may be well expressed by the following interpolation formula of Prandtl:

$$\frac{l}{r} = 0.14 - 0.08 \left(1 - \frac{y}{r}\right)^2 - 0.06 \left(1 - \frac{y}{r}\right)^4 \quad (13)$$

It turns out that the above distribution of the non-dimensional mixing length holds not only for round pipes but also for channels with parallel walls. This is shown by the tests of Nikuradse and Fritsch (references 4 and 7). Figure 7 shows the results of these tests. For the value of  $r$  half the channel width is taken. This distribution holds moreover for rough round pipes (reference 9) (fig. 19).

A consideration of the work of Doench (reference 2) and Nikuradse (reference 7) shows that for the case of diffuser with plane walls the same type of dependence for the mixing length is obtained and, what is of particular importance, we have the same value of the nondimensional mixing length at the axis (outer edge of the boundary layer). Figures 8 and 9 show the distribution of the non-dimensional mixing length in plane-wall diffusers as obtained from the tests of Doench (fig. 8) and Nikuradse (fig. 9) for various angles of divergence. For plane converging passages, however, a different type of mixing length distribution is obtained.

Strictly speaking, for plane-wall diffusers figure 9 shows a certain dependence of the mixing length on the angle of divergence of the diffuser and therefore on the pressure gradient. Bearing in mind, however, that for an angle of divergence  $\alpha = 0^\circ$  the pressure gradient is already negative, it follows that the effect of the pressure gradient on the mixing length distribution at positive or small negative gradients is comparatively small and in any case less than the effect of the pressure gradient on the velocity distribution.<sup>1</sup>

---

<sup>1</sup> Yamamoto expressed the relation between the mixing length and the distance from the wall for smooth round pipes by the formula (reference 6)

$$\frac{l}{r} = 0.14 \left[1 - \left(\frac{y}{r}\right)^2\right] \left[1 + \frac{1}{3} \left(\frac{y}{r}\right)^2\right]$$

which gives results differing very little from those obtained by the Prandtl formula.

Thus, the nondimensional mixing length may be looked upon as a more general and more fundamental magnitude as compared with the velocity profile and may be considered as approximately the same for a larger class of boundary layers. On the other hand, we must admit that the effect of the pressure gradient on the shear profile is quite large. In fact, the shear profile shown on figure 4 for the case  $\frac{\partial p}{\partial s} > 0$  corresponding to the conditions at the upper surface of a wing at an angle of attack of  $12^\circ$  is very different from the shear profile for the case  $\frac{\partial p}{\partial s} = 0$  for the same shear at the wall.

On the basis of the above data, it may be stated that for positive or small negative pressure gradients the mixing length distribution may be considered as depending only on the nondimensional distance from the wall and the difference in the velocity profiles as due only to the difference in the shear stresses. With the above assumption we can at once explain the difference in the characteristic appearance of the velocity distribution for a small positive pressure gradient and a negative pressure gradient, respectively. For the same distribution of the nondimensional mixing length the derivative of the velocity with respect to  $y$  according to formula (12) will in fact increase with increasing shear stress  $\tau$ . The latter, however, for the same nondimensional distance from the wall is larger the larger the pressure gradient (fig. 10). Hence it follows that for positive pressure gradients the velocity distribution will be different from that for zero pressure gradient.

Applying the Prandtl formula of the mixing length distribution to the external problem, we easily obtain the laws of variation of the velocity transverse to the boundary layer. The formula is rewritten in the following form

$$\frac{l}{\delta} = 0.14 - 0.08 \left(1 - \frac{y}{\delta}\right)^2 - 0.06 \left(1 - \frac{y}{\delta}\right)^4 \quad (13')$$

5. Employing formula (12), we obtain the following differential equation:

$$dU = \sqrt{\frac{\tau}{\rho}} \frac{1}{l} dy = \sqrt{\frac{\tau}{\rho}} \frac{1}{\left(\frac{l}{\delta}\right)} d\left(\frac{y}{\delta}\right) \quad (14)$$

Integrating, we have:

$$U = \int \sqrt{\frac{\tau}{\rho}} \frac{1}{\left(\frac{l}{\delta}\right)} d\left(\frac{y}{\delta}\right) + C$$

The arbitrary constant of integration is determined by the condition that for  $\frac{y}{\delta} = 1$ ;  $\tau = 0$ ,  $U = U_{\delta}$  so that  $C = U_{\delta}$  and

$$U = U_{\delta} + \int \sqrt{\frac{\tau}{\rho}} \frac{1}{\left(\frac{l}{\delta}\right)} d\left(\frac{y}{\delta}\right) \quad (15)$$

The above expression may also be written in the form

$$U = U_{\delta} + \int_1^{y/\delta} \sqrt{\frac{\tau}{\rho}} \frac{1}{\left(\frac{l}{\delta}\right)} d\left(\frac{y}{\delta}\right) \quad (15')$$

Substituting in (15) the values of  $\tau$  and  $l/\delta$  from equations (1) and (13), we shall have:

$$U = U_{\delta} + \sqrt{\frac{\tau_0}{\rho}} \int_1^{y/\delta} \frac{\sqrt{1 + A_1 \left(\frac{y}{\delta}\right) + A_2 \left(\frac{y}{\delta}\right)^2 + \dots}}{0.14 - 0.03 \left(1 - \frac{y}{\delta}\right)^2 - 0.06 \left(1 - \frac{y}{\delta}\right)^4} d\left(\frac{y}{\delta}\right) \quad (16)$$

since  $A_0$  is always equal to 1. Using for  $\tau$  the combination of conditions (I), (II), (III), (IV), and (V) or the combination (I), (II), (III), and (IV) the integral on the right of equation (16) is reduced to an elliptic integral of the second kind. In particular, using conditions (I), (II), (III), (IV), and (V) expression (16) assumes the following form:

$$U = U_{\delta} + \sqrt{\frac{\tau_0}{\rho}} \int_1^{y/\delta} \frac{\sqrt{1 + A_1 \left(\frac{y}{\delta}\right) + A_3 \left(\frac{y}{\delta}\right)^3 + A_4 \left(\frac{y}{\delta}\right)^4}}{0.14 - 0.08 \left(1 - \frac{y}{\delta}\right)^2 - 0.06 \left(1 - \frac{y}{\delta}\right)^4} d\left(\frac{y}{\delta}\right) \quad (17)$$

Using for  $\tau$  the conditions (I), (II), and (III) the integral at the right of equation (16) assumes the following finite form:

$$U = U_{\delta} + \sqrt{\frac{\tau_0}{\rho}} \int_1^{y/\delta} \frac{\sqrt{1 + A_1 \left(\frac{y}{\delta}\right) + A_2 \left(\frac{y}{\delta}\right)^2}}{0.14 - 0.08 \left(1 - \frac{y}{\delta}\right)^2 - 0.06 \left(1 - \frac{y}{\delta}\right)^4} d\left(\frac{y}{\delta}\right) \quad (18)$$

Figures 11, 12, and 13 give the velocity distribution for three sections of the boundary layer at the upper surface of a wing according to the tests of Gruschwitz for an angle of attack of  $12^\circ$ . These three sections are near the point of separation and the velocity profiles are therefore of particular interest. The velocity profiles for the same sections computed from formulas (17) and (18) give a sufficiently good agreement with the experimental profiles. For comparisons there are also given the velocity profiles based on the von Kármán formula for straight round tubes:

$$U = U_\delta + \frac{\sqrt{\frac{\tau_0}{\rho}}}{\kappa} \left[ \ln \left( 1 - \sqrt{1 - \frac{y}{\delta}} \right) + \sqrt{1 - \frac{y}{\delta}} \right] \quad (19)$$

where  $\kappa$  is a constant approximately equal to 0.4.

The velocity profiles based on formula (17) agree better with experiment than those based on formula (18) - a fact that may be explained by the more close approximation of the shear given by (17) as compared with (18). The less favorable agreement of the theoretical with the experimental velocity profiles at the section  $x = 27.05$  cm is evidently explained by the fact that the section is not entirely in the turbulent boundary region. As a matter of fact, this section still lies in the region where the shear at the wall increases in the direction from leading to trailing edge, i.e., in the region of transition. Combinations of conditions (I), (II), (III), and (IV) or (I), (II), (III), and (V) give a less good agreement between the theoretical and experimental distributions than conditions (I), (II), (III), (IV), and (V) or even conditions (I), (II), and (III).

Figures 14, 15, 16, 17, and 18 give the velocity profiles at five sections of the boundary layer of a symmetrical Joukowski airfoil at an angle of attack  $\alpha = -0.18^\circ$  according to the tests of Fage and Falkner (reference 3). The velocities computed from formulas (17) and (18) and also from the von Kármán formula are likewise given on the figures for the same sections. The agreement of the test curves with those computed from (17) and (18) may be considered as satisfactory.

Notwithstanding the fact that the static pressure gradient is small, the difference between the curves computed from (17) and (18) and the curve of von Kármán is

rather considerable. It is therefore expedient to take into account the conditions of the external problem in obtaining the velocity profiles even at small static pressure gradients.

The good agreement with experiment of the velocity profiles in the turbulent boundary layer of a wing makes it possible, in the first place, to proceed to the solution of the very important problem of the separation of the turbulent boundary layer, and in the second place to compute correctly the resistance of the surface roughness in the boundary layer.

6. Let us introduce, analogous to the "friction velocity" of Prandtl

$$v_* = \sqrt{\frac{\tau_0}{\rho}} \quad (20)$$

the corresponding magnitude for the pressure acting on a cross section of the boundary layer and denote this magnitude by  $p_*$ . We shall then have:

$$p_* = \sqrt{\frac{\delta}{\rho} \frac{\partial p}{\partial S}} \quad (21)$$

The above expression may be denoted as the "pressure velocity." Using (20) and (21), the integral of equation (18) may be written as follows:

$$\begin{aligned}
 U = U_\delta + 14.3 \frac{(2v_*^2 + p_*^2)^a}{(v_*^2 + p_*^2)^{\frac{3}{2}}} & \left[ L_1 \ln \frac{\left( \frac{v_*^2}{v_*^2 + p_*^2} + \frac{y}{\delta} \right)^{-\frac{1}{2}} - \left( \frac{v_*^2}{v_*^2 + p_*^2} \right)^{\frac{1}{2}}}{\left( \frac{v_*^2}{v_*^2 + p_*^2} + \frac{y}{\delta} \right)^{\frac{1}{2}} + \left( \frac{v_*^2}{v_*^2 + p_*^2} \right)^{\frac{1}{2}}} \right. \\
 & + \frac{M_2}{2} \ln \frac{\frac{v_*^2}{v_*^2 + p_*^2} + \frac{y}{\delta} - 2E \left( \frac{v_*^2}{v_*^2 + p_*^2} + \frac{y}{\delta} \right)^{\frac{1}{2}} + D}{\frac{v_*^2}{v_*^2 + p_*^2} + \frac{y}{\delta} + 2E \left( \frac{v_*^2}{v_*^2 + p_*^2} + \frac{y}{\delta} \right)^{\frac{1}{2}} + D} \\
 & \left. + G \operatorname{arc tan} \frac{F \left( \frac{v_*^2}{v_*^2 + p_*^2} + \frac{y}{\delta} \right)^{\frac{1}{2}}}{D - \left( \frac{v_*^2}{v_*^2 + p_*^2} + \frac{y}{\delta} \right)} + H \operatorname{arc tan} P \left( \frac{v_*^2}{v_*^2 + p_*^2} + \frac{y}{\delta} \right) \right] \quad (22)
 \end{aligned}$$

where the coefficients  $L_1, M_2, D, E, F, G, H, P$  are non-dimensional magnitudes depending only on  $v_*^2$  and  $p_*^2$ . Since in deriving (22) the laminar sublayer was not taken into account, this formula, which is similar to the von Kármán formula:

$$U = U_\delta + \frac{v_*}{\kappa} \left[ \ln \left( 1 - \sqrt{1 - \frac{y}{\delta}} \right) + \sqrt{1 - \frac{y}{\delta}} \right] \quad (19)$$

and the Prandtl-Nikuradse formula:

$$U = U_\delta + \frac{v_*}{\kappa} \ln \frac{y}{\delta} \quad (23)$$

does not, of course, satisfy the condition at the wall, since for  $\frac{y}{\delta} = 0$ , we have  $U = -\infty$ .

7. In the special case of a flat plate, i.e., for  $\frac{dp}{ds} = 0$ , the coefficients of series (1) assume the following values:

a) Using the combination of conditions (I), (II), (III), (IV), and (V):

$$A_0 = 1; \quad A_1 = 0; \quad A_2 = 0; \quad A_3 = -4; \quad A_4 = 3 \quad (4')$$

b) Using combination of conditions (I), (II), and (III):

$$A_0 = 1; \quad A_1 = 0; \quad A_2 = -1 \quad (6')$$

Thus for this particular case, expressions (17) and (18) assume the following form:

$$U = U_\delta + v_* \int_1^{y/\delta} \frac{\sqrt{1 - 4 \left(\frac{y}{\delta}\right)^3 + 3 \left(\frac{y}{\delta}\right)^4}}{0.14 - 0.08 \left(1 - \frac{y}{\delta}\right)^2 - 0.06 \left(1 - \frac{y}{\delta}\right)^4} d\left(\frac{y}{\delta}\right) \quad (17')$$

$$U = U_\delta + v_* \int_1^{y/\delta} \frac{\sqrt{1 - \left(\frac{y}{\delta}\right)^2}}{0.14 - 0.08 \left(1 - \frac{y}{\delta}\right)^2 - 0.06 \left(1 - \frac{y}{\delta}\right)^4} d\left(\frac{y}{\delta}\right) \quad (18')$$

Figure 19 gives the plot of equations (17') and (18') using as coordinates  $\frac{U_\delta - U}{v_*}$  and  $\frac{y}{\delta}$ . The same figure shows for comparison the curves corresponding to the von Kármán and Prandtl-Nikuradse formulas.

The author expresses his deep gratitude to Professor Loytsansky for a number of important suggestions in connection with the above work. All the computations were carefully carried out by the engineers, P. E. Kuryatnikoff and S. S. Jacobson, to whom the author expresses his grateful acknowledgment.

## REFERENCES

1. Buri, A.: Eine Berechnungsgrundlage fuer die turbulente Grenzschicht bei beschleunigter und verzögerteter Grundstroemung. Promotion arbeit. Buchdruckerai A. G. Jean Frey. Zurich, 1931.
2. Doench, E.: Divergente und konvergente turbulente Stroemungen mit kleinen Oeffnungswinkeln. Forschungsarbeiten auf dem Gebiete des Ingenieurwesens, Heft 282, Berlin, 1926.
3. Fage, A., and Falkner, V. M.: An Experimental Determination of the Intensity of Friction on the Surface of an Aerofoil. R. & M. No. 1315, British A.R.C., 1931.
4. Fritsch, Walter: Der Einfluss der Wandrauhigkeit auf die turbulente Geschwindigkeitsverteilung in Rinnen. Z.f.a.M.M., Band 8, Heft 3, 1928, p. 215.
5. Gruschwitz, E.: Die Turbulente Reibungsschicht in ebener Stroemung bei Druckabfall und Druckanstieg. Göttingen Dissertation, Ingenieur-Archiv, II Band, 3 Heft, 1931.
6. Yamamoto, Tsunayuki: Study of Turbulent Flow in Smooth Pipes. Jour. of the Society of Mechanical Engineers, Japan, vol. 37, no. 212, December 1934.
7. Nikuradse, J.: Untersuchungen über die Stroemungen des Wassers in konvergenten und divergenten Kanaelen. Forschungen aus dem Kaiser Wilhelm-Institut fuer Stroemungsforschung, no. 289, Berlin, 1921.
8. Nikuradse, J.: Gesetzmaessigkeiten der turbulenten Stroemung in glatten Rohren. Forschungsheft no. 356, Berlin, 1932.
9. Nikuradse, J.: Stroemungsgesetz in rauhen Rohren. Forschungsheft no. 361, Berlin, 1933.

x Distance of a section from the leading edge measured along the contour of the upper surface.

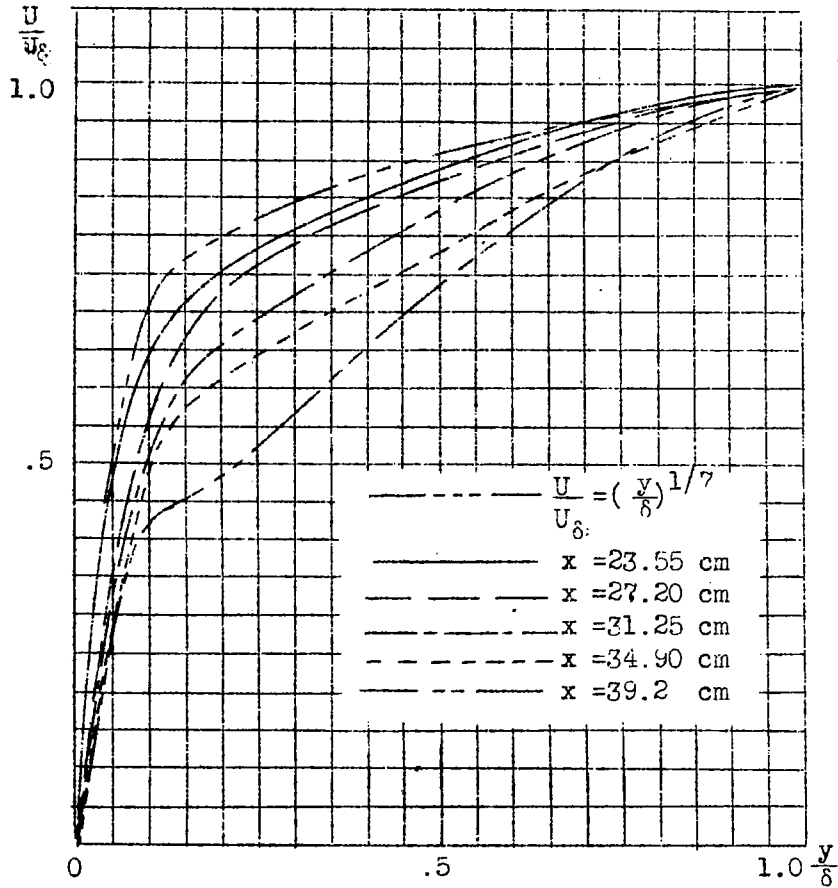


Figure 1.- Wing with Gottingen 397 profile.  
 ( $\alpha = 6^\circ$ , chord  $t = 40$  cm.).

x' Distance from entrance.

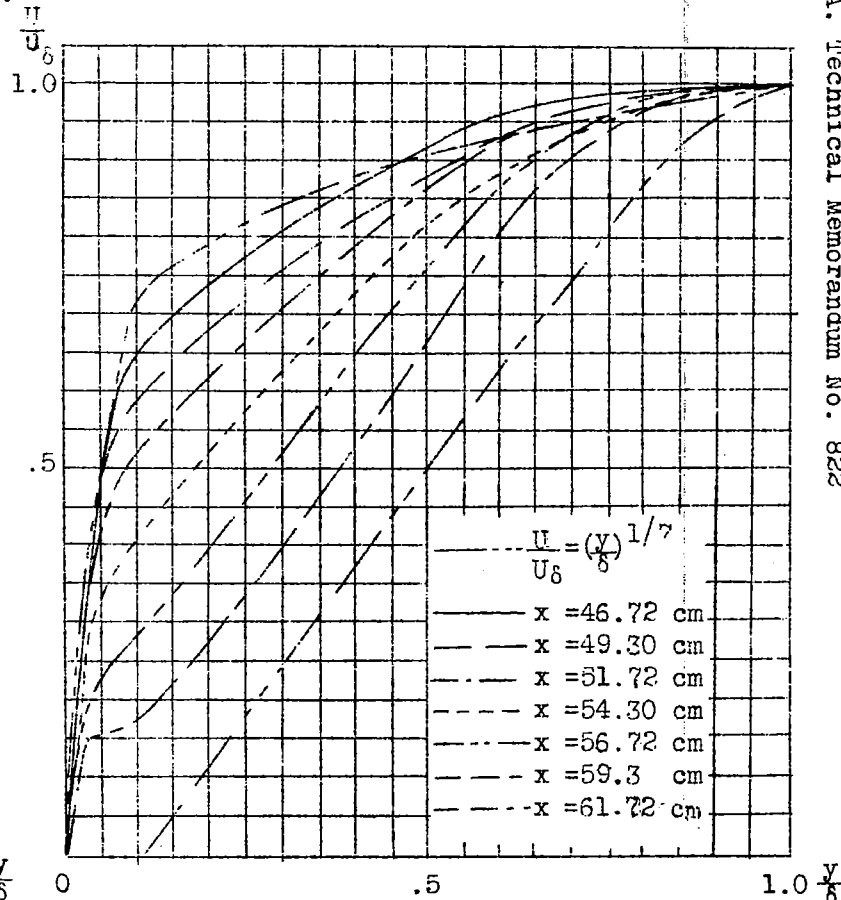


Figure 2.- Boundary layer of diffuser of profile section 3.

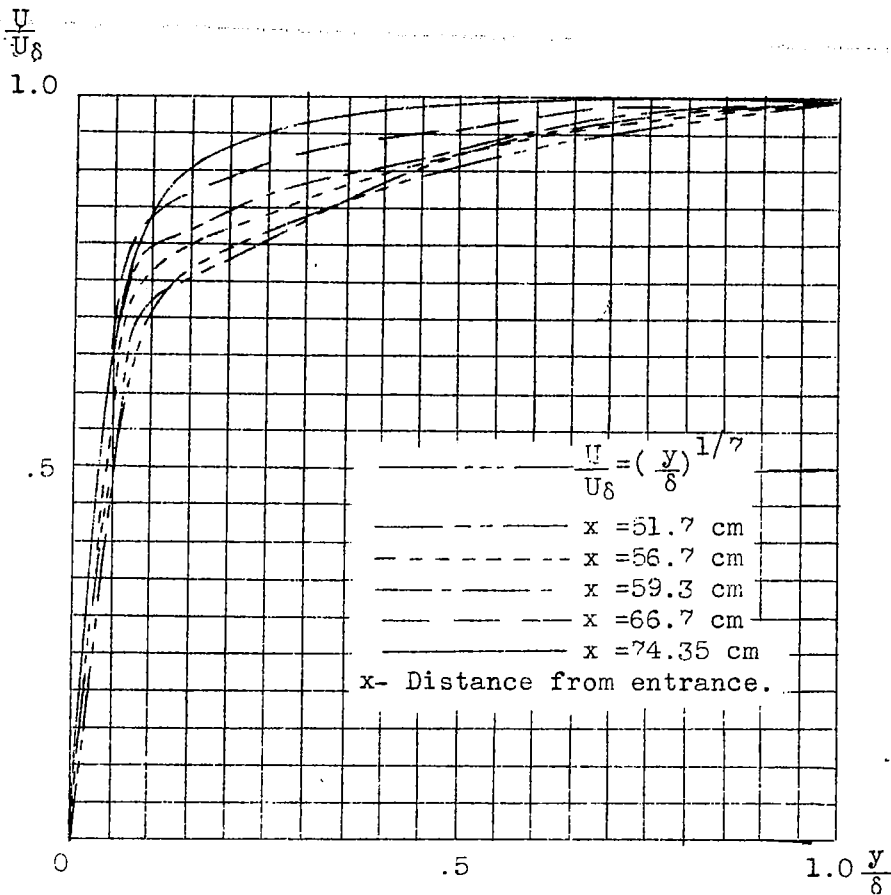


Figure 3.- Boundary layer of diffuser of profile section 5.

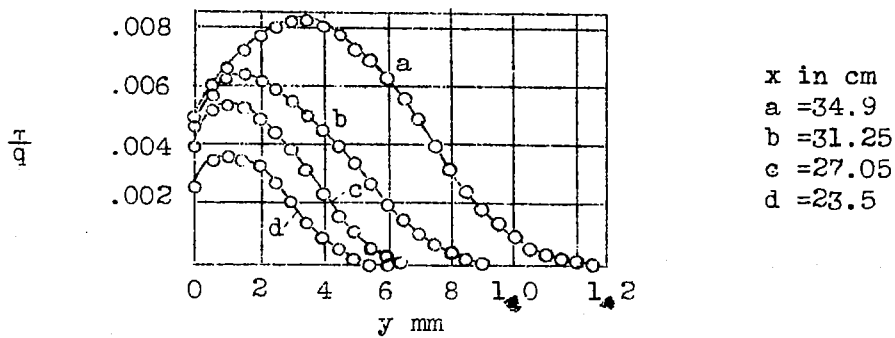


Figure 5.

\_\_\_\_\_  $\frac{dp}{dS} = 330.9 \frac{kg}{m^3}; \frac{\tau}{\tau_0} = 1 + A_1 \left(\frac{y}{\delta}\right) + A_2 \left(\frac{y}{\delta}\right)^2$   
 - - - - -  $\frac{dp}{dS} = 330.9 \frac{kg}{m^3}; \frac{\tau}{\tau_0} = 1 + A_1 \left(\frac{y}{\delta}\right) + A_3 \left(\frac{y}{\delta}\right)^3 + A_4 \left(\frac{y}{\delta}\right)^4$   
 - - - - -  $\frac{dp}{dS} = 0; \frac{\tau}{\tau_0} = 1 + A_1 \left(\frac{y}{\delta}\right) + A_2 \left(\frac{y}{\delta}\right)^2$   
 - - - - -  $\frac{dp}{dS} = 0; \frac{\tau}{\tau_0} = 1 + A_1 \left(\frac{y}{\delta}\right) + A_3 \left(\frac{y}{\delta}\right)^3 + A_4 \left(\frac{y}{\delta}\right)^4$

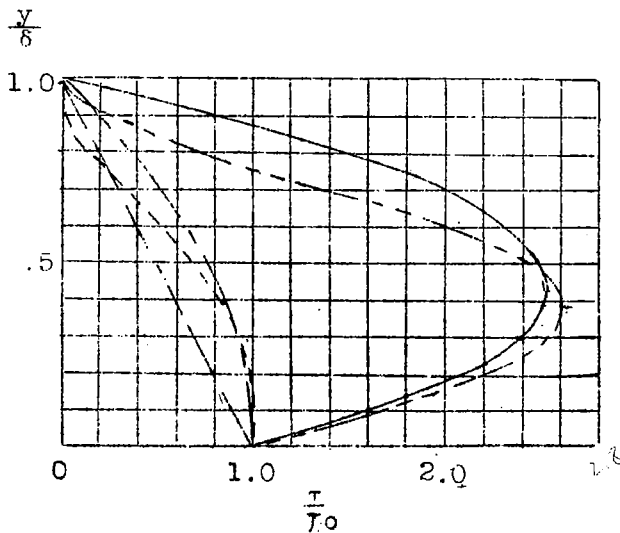


Figure 4.

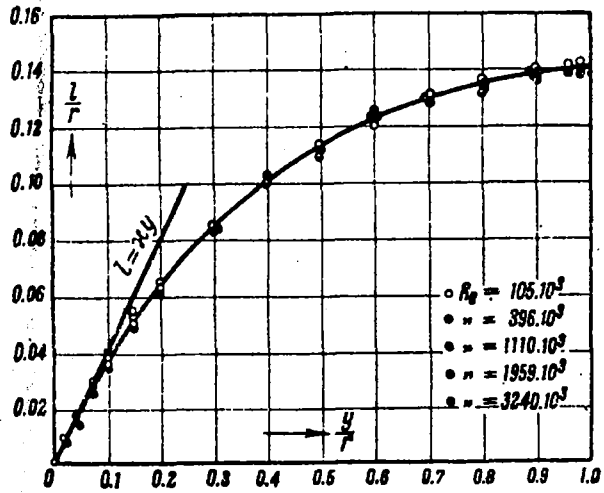


Figure 6

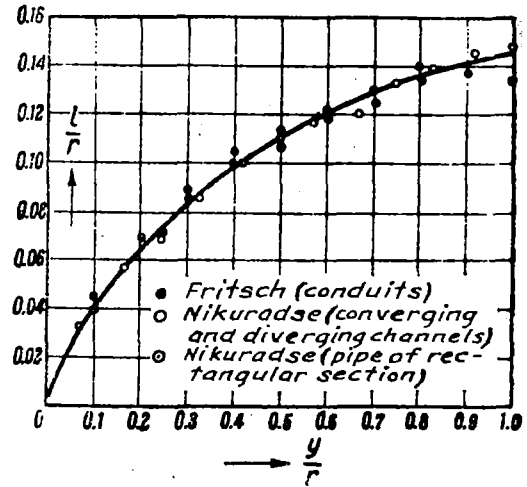


Figure 7

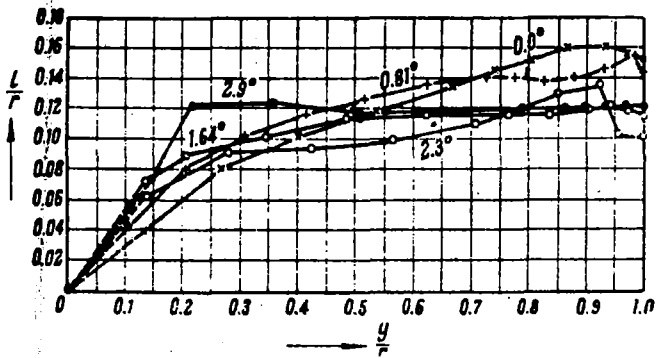


Figure 8

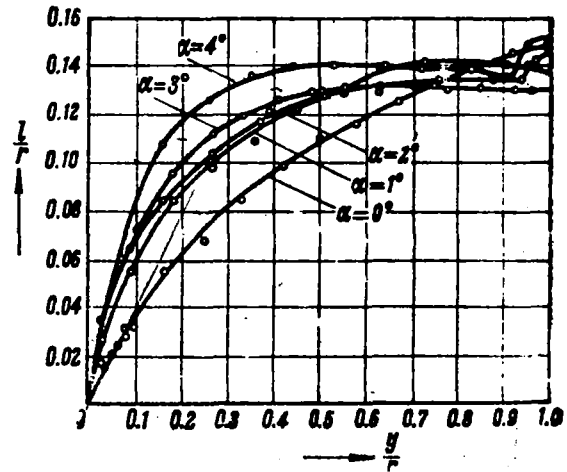


Figure 9

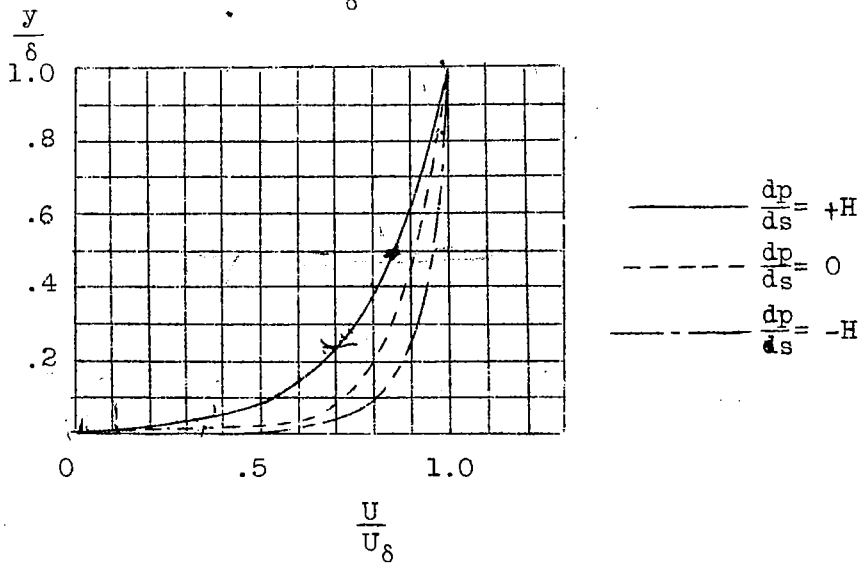
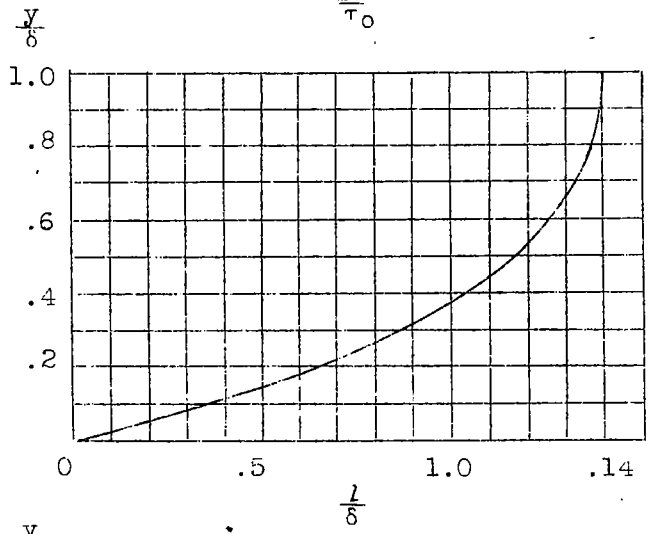
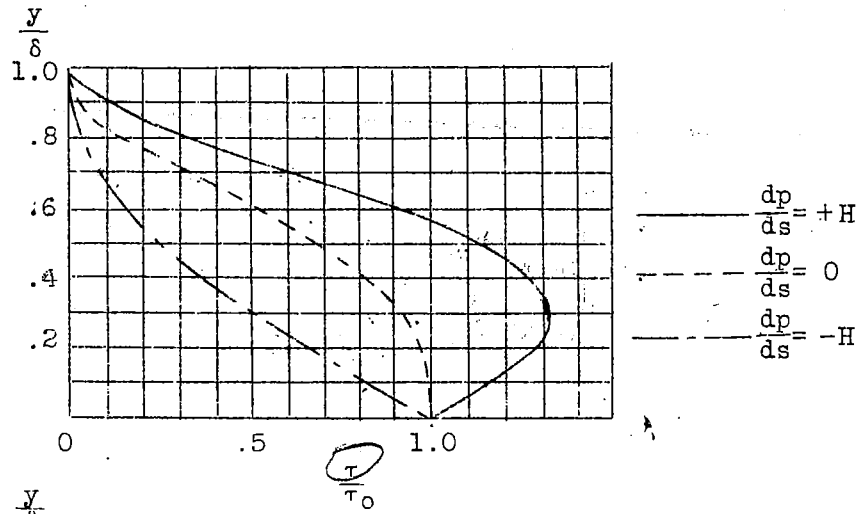


Figure 10.

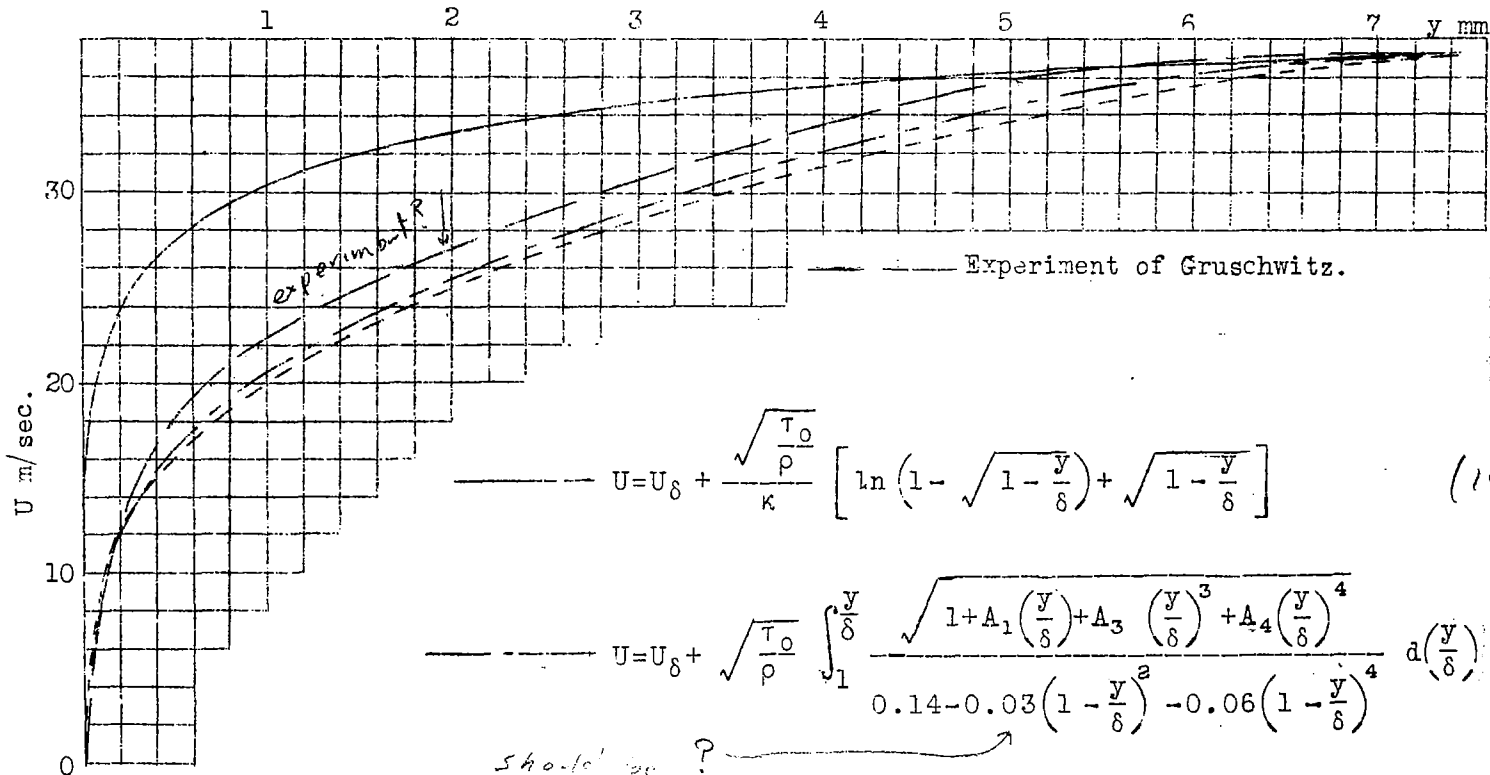


Figure 11.- Wing with Gottingen 397 profile ( $t = 40$  cm.  $\alpha = 12^\circ$ ,  $x = 27.05$  cm.  $\delta = 0.0075$  m.  $\tau_0 = 0.3278$  kg/m<sup>2</sup>;  $dp/ds = 233$  kg/m<sup>3</sup>.)

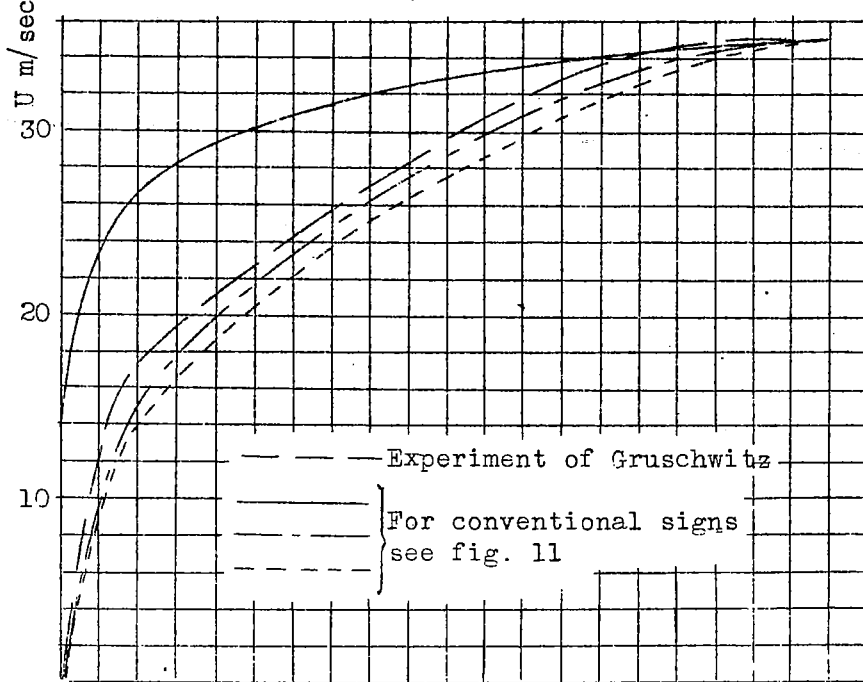


Figure 12.- Wing with Gottingen 397 profile ( $\alpha = 12^\circ$ ,  $x = 31.24$  cm.,  $\delta = 0.009975$  m.,  $\tau_0 = 0.3405$  kg/m<sup>2</sup>,  $dp/ds = 254$  kg/m<sup>3</sup>.)

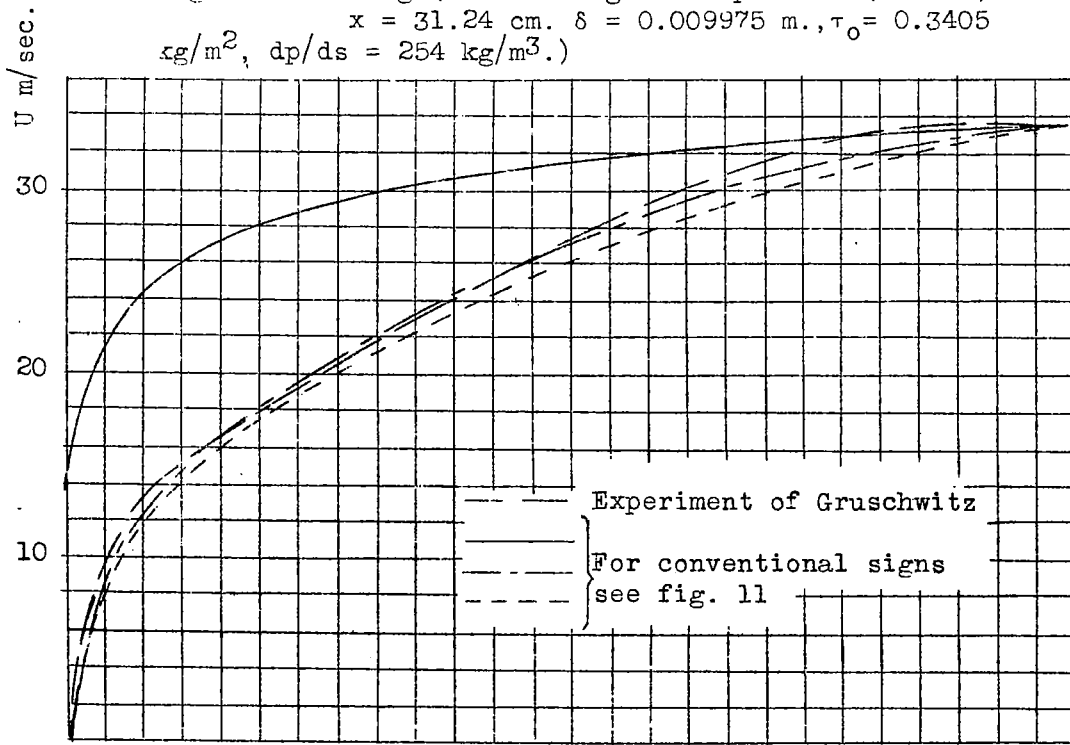


Figure 13.- Wing with Gottingen 397 profile ( $\alpha = 12^\circ$ ,  $x = 34.9$  cm.,  $\delta = 0.013$  m.,  $\tau_0 = 0.314$  kg/m<sup>2</sup>;  $dp/ds = 187$  kg/m<sup>3</sup>.)

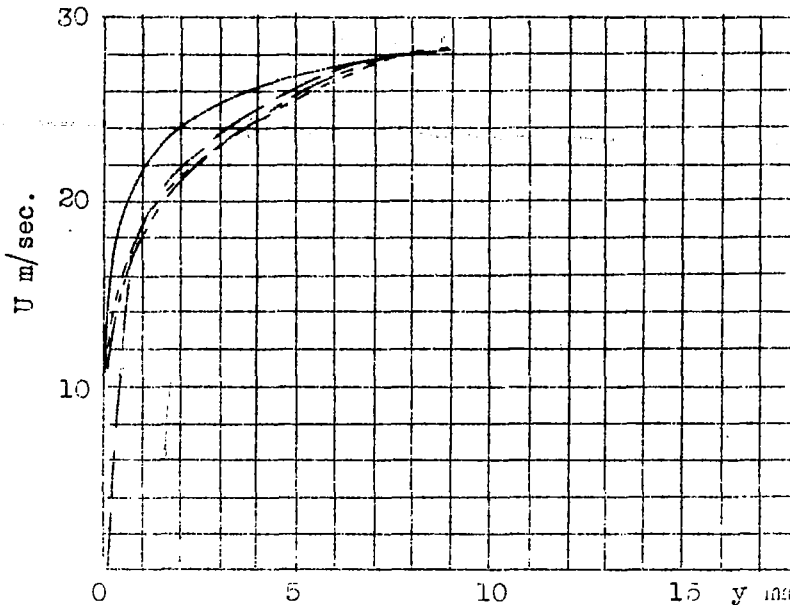


Figure 14.- Symmetrical Joukowski airfoil with maximum thickness 15% of chord ( $x = 0.508$  m. ( $x/t = 0.504$ ),  $\delta = 0.00905$  m.,  $\tau_0 = 0.198$  kg/m<sup>2</sup>,  $dp/ds = 7.26$  kg/m<sup>3</sup>.)

— — — Experiment of Fage and Falmer.  
 ————— } For conventional signs  
 - - - - - } see fig. 11  
 - - - - - }

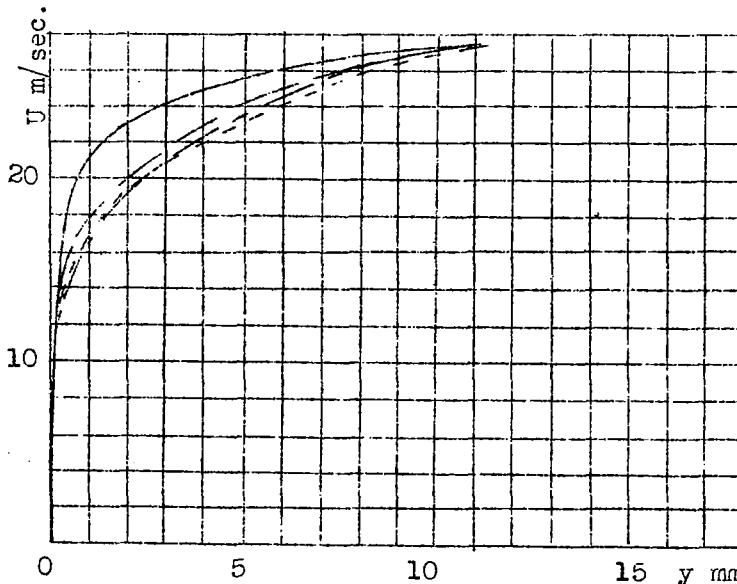


Figure 15.- Symmetrical Joukowski airfoil with maximum thickness 15% of chord ( $t = 1.009$  m.,  $\alpha = 0^\circ$ ,  $x = 0.610$  m., ( $x/t = 0.605$ ),  $\delta = 0.01145$  m.;  $\tau_0 = 0.1741$  kg/m<sup>2</sup>,  $dp/ds = 18.6$  kg/m<sup>3</sup>.)

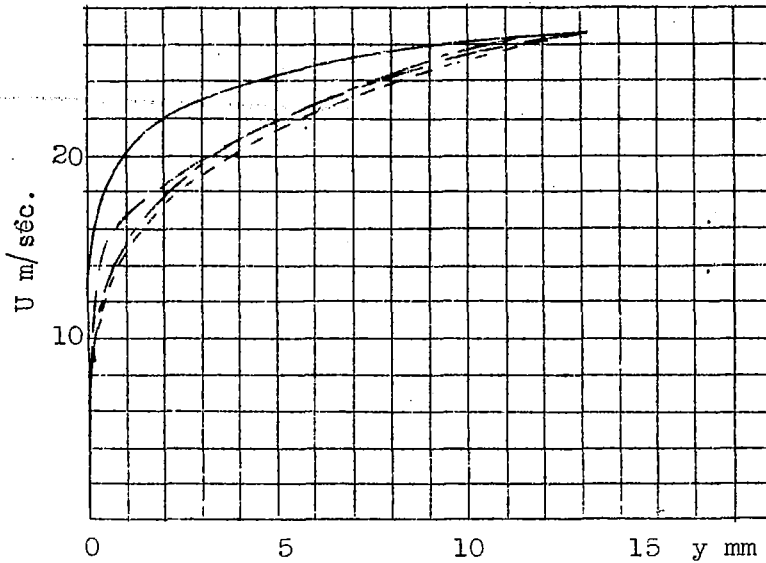


Figure 16.- Symmetrical Joukowski airfoil with maximum thickness 15% of chord ( $x = 0.7119$  m., ( $x/t=0.706$ ),  $\delta = 0.0136$  m.,  $\tau_0 = 0.1659$  kg/m<sup>2</sup>,  $dp/ds = 19.34$  kg/m<sup>3</sup>.)

— + — Experiment of Fage and Falkner  
 ————— } For conventional signs  
 - - - - - } see fig. 11

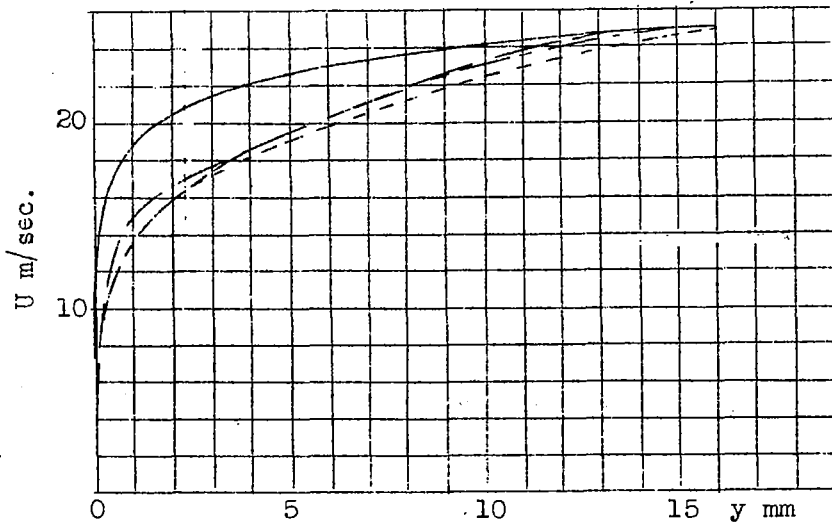


Figure 17.- Symmetrical Joukowski airfoil with maximum thickness 15% of chord ( $x = 0.8135$  m., ( $x/t = 0.807$ )  $\delta = 0.0166$  m.,  $\tau_0 = 0.1154$  kg/m<sup>2</sup>,  $dp/ds = 19.3$  kg/m<sup>3</sup>.)

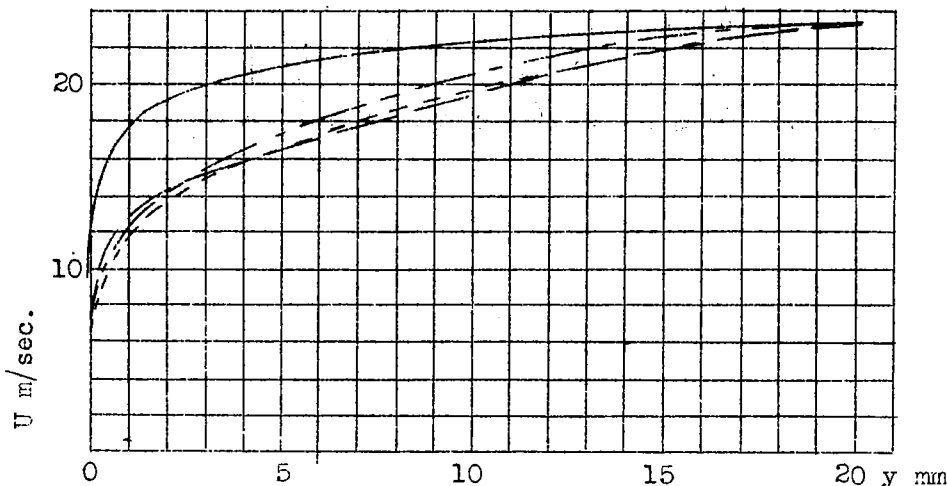


Figure 18.- Symmetrical Joukowski airfoil with maximum thickness 15% of chord ( $\bar{x} = 0.964$  m., ( $x/t = 0.956$ ),  $\delta = 0.0202$  m.  $\tau_0 = 0.09445$  kg/m<sup>2</sup>,  $dp/ds = 23.25$  kg/m<sup>3</sup>.)

— — — Experiment of Fage and Falkner

For conventional signs see fig. 11

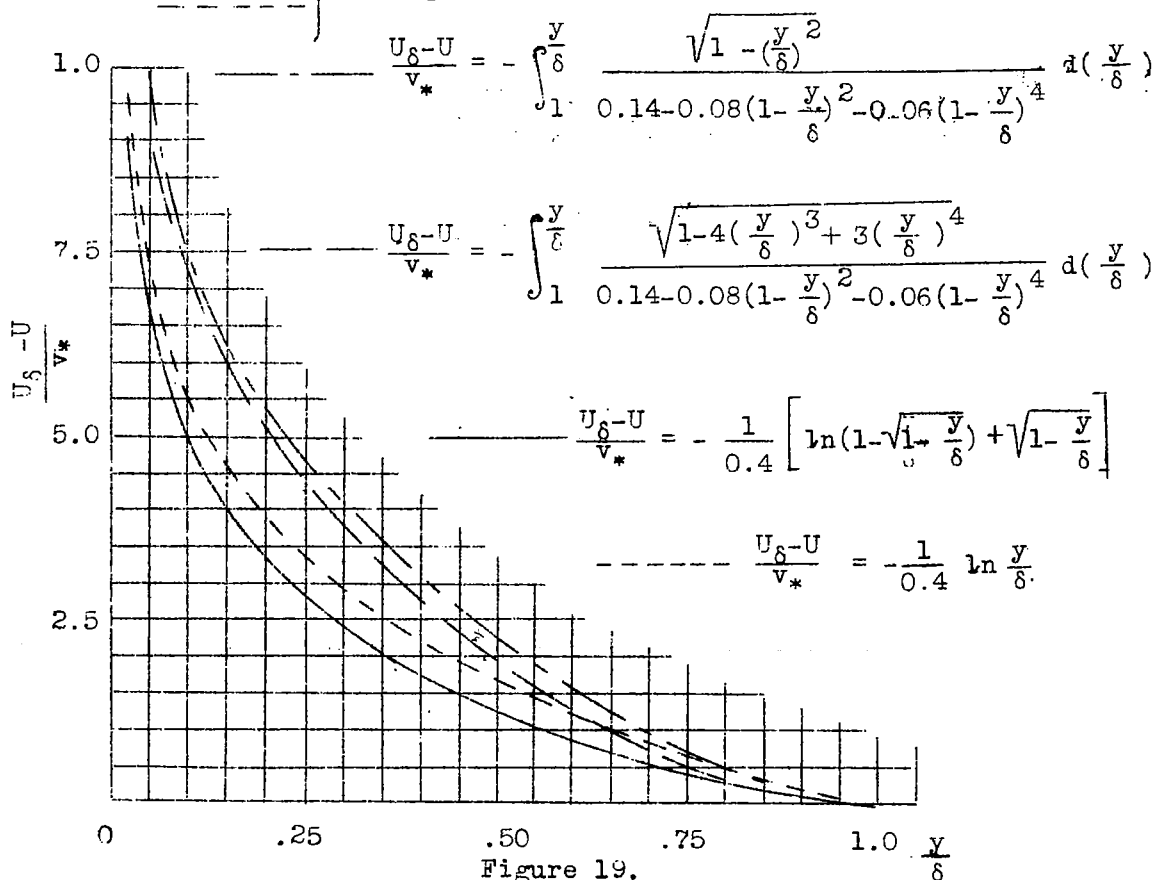


Figure 19.

30  
1/31/50

NASA Technical Library



3 1176 01437 4202

6.0

6.0

